TIMODAZ PROJECT

SCOPING CALCULATIONS

RESULTS FROM CIMNE

July, 2007

CIMNE
www.cimne.upc.es

CIMNE Edificio C1, Campus Norte UPC C/ Gran Capitán S/N 08034 Barcelona, España
Tel.(+34) - 93 401 7441 / 93 205 7016 /Fax.(+34) 93 401 6517
e-mail: antonio.gens@upc.edu

TABLE OF CONTENTS

1. INTRODUCTION

During the review of the TIMODAZ project, the participant groups were asked to clarify how the present project can achieve the estimation of the ultimate thermal limits of the clays in the context of the long term performance of the repository design. As discussed and proposed in the meeting held at Liege, some scoping calculations have been performed by some groups to study some relevant aspects.

The objective of this scoping calculations is to study, numerically, the THM responses of the host formations under different conditions and thus to have an insight on the most critical conditions (and key factors) for the behaviour of the host formations including their thermal limits.

In our scoping calculations only the behaviour of plastic clay (PC) has been investigated. The host formation is studied in three different conditions: heating in drained, undrained and dripping cases by applying the VHLW thermal source after 50 years of cooling time on surface. The other thermal source, MOX50, is applied for the drained case after 50 years of cooling time on surface. During the calculations; due to some uncertainties on some parameters (such as thermal conductivity of PC) additional analyses have been performed to try to clarify those uncertainties.

2. CONCEPTUAL MODELLING and DESIGN

2.1 Constitutive Models

In the calculations thermal elasticity model is used in the constitutive equations. The formulations and PC clay parameters used in the constitutive model are given below:

The strains due to change of temperature are assumed purely volumetric according to:

$$\Delta\varepsilon_V = 3b_s\Delta T \quad (\Delta\varepsilon_v > 0, \text{ extension};\ \Delta\varepsilon_v < 0, \text{ compression}) \qquad \text{(Eq.2.1)}$$

where;

b_s	$^oC^{-1}$	Linear thermal expansion coefficient for the medium

The PC parameters are:

Geomechanical parameters		PC
Young's elastic modulus [MPa]	E'	300
Poisson's ratio [-]	υ'	0.125

Table 2.1 : Geomechanical parameters

Hydraulic parameters		PC
Porosity	n	0.39
Intrinsic Permeability [m^2]	$(K_{ii})_o$	1.10^{-18}

Table 2.2 : Hydraulic parameters

Thermal parameters		PC
Thermal conductivity [W/(mK)]	λ	1.5
Linear thermal expansion coefficient [K^{-1}]	b_s	10^{-5}
Heat specific capacity of the sold [J/kg/K]	C_s	874

Table 2.3 : Thermal parameters

2.2 Geometry

The repository is simulated according to axi-symmetry and plane strain conditions which are idealization of excavations of a cylindrical cavity in an infinite medium. The AB surface represents the tunnel surface of the gallery. The inner radius of the gallery R_0 is equal to 2 m and the outer radius is chosen as 200 m (100 times of the inner radius).

The domain is discretized by 600 quadrilateral isotropic elements. The geometry of the analysis is given in the following figure:

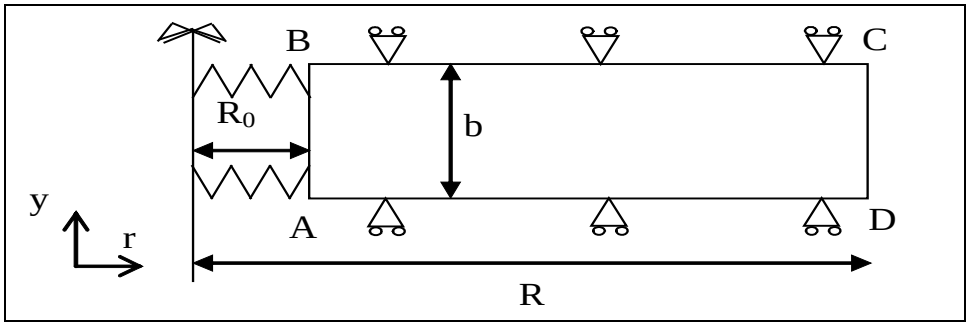

Figure 2.1 Geometry of the repository

where;

$b = 1$ m
$R_0 = 2$ m
$R = 200$ m

2.3 Initial Conditions

The clay formation around the gallery is considered homogeneous and isotropic. Initial Stresses and Pore Pressure used in the calculations are given in Table 2.4. In addition, the modeling zone is supposed to be sufficiently deep so that the variation of the stress and pore pressure with depth is neglected. The formation is assumed to be completely saturated.

Initial state		**PC**
Total stresses [MPa]	σ_H	4.5
	σ_v	4.5
Pore pressure [MPa]	P_{w0}	2.25
Effective stresses [MPa]	σ'_H	2.25
	σ'_v	2.25
Temperature [°C]	T_0	16

Table 2.4 : Initial State : Initial Stress, pore water pressure and temperature

2.4 Boundary Conditions

Mechanical boundary conditions are prescribed such as:

- The vertical displacements are blocked on the faces AD and BC.
- On the face CD;

  $\sigma_r = \sigma_H = \sigma_v$

Hydraulic boundary conditions are prescribed such as:

- Impermeable on the face AD and BC
- $P_w = P_{w0}$ on the face CD

Thermal boundary conditions are prescribed such as:

- Adiabatic on the face AD and BC
- $T = T_0$ on the face CD

2.5 Thermal Source Terms

The two thermal source terms studied in the scoping calculations. **VHLW** for all cases and **MOX50** for drained case to compare with the former one. All these two wastes are applied considering **50** years of cooling time on the surface (Reference case).

The heat fluxes of these two wastes after their production are given in the Figure 2.2.

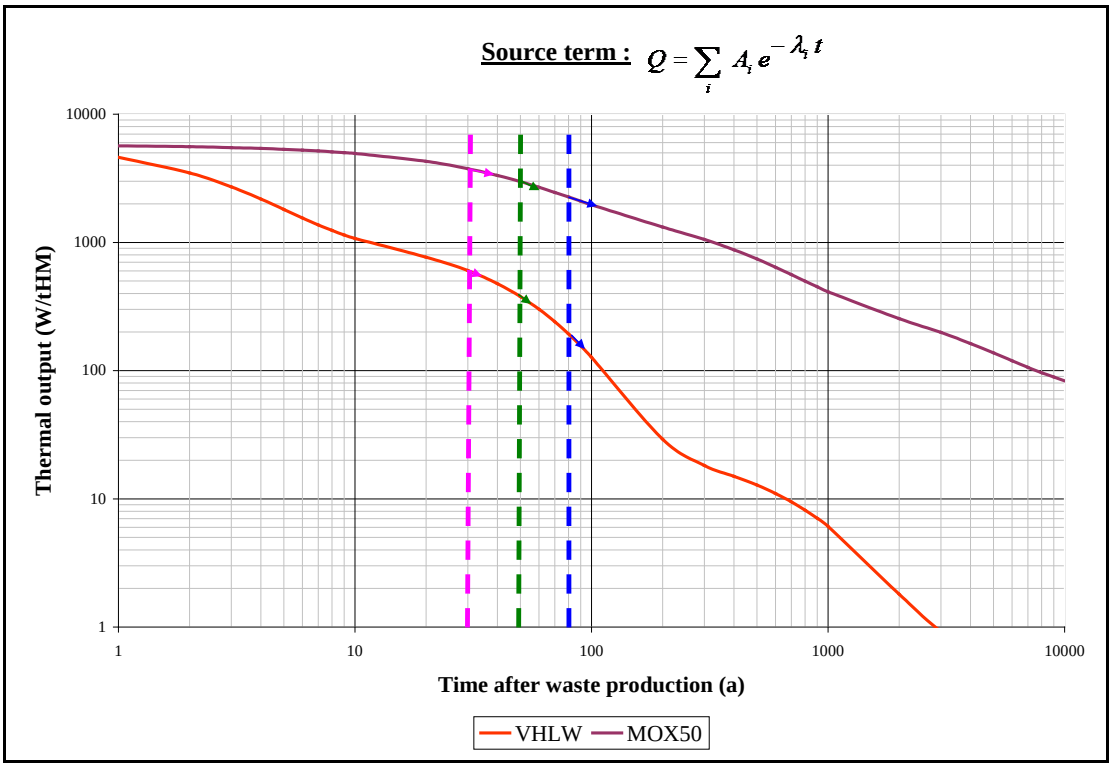

Figure 2.2: Time evolution of heat flux (W/tHM) of two kinds of wastes after their production

The heat production of the wastes is calculated by the following equation:

$$Q = \sum_i A_i e^{-\lambda_i t} \qquad \text{(Eq.2.2)}$$

where Q is expressed in W/tHM and t in years.
Note: tHM (tonnes Heavy Metal) refers to the initial mass of the wastes.

The corresponding parameters for two types of wastes are listed in table 2.5 and 2.6.

VHLW				
A_1	A_2	A_3	A_4	A_5
5021	1205	27.04	0.7576	0.1
λ_1	λ_2	λ_3	λ_4	λ_5
0.3894	0.02458	1.63×10^{-3}	6.546×10^{-5}	0

Table 2.5: Parameters for VHLW waste

MOX50			
A_1	A_2	A_3	A_4
3782	1545	326.4	100.6
λ_1	λ_2	λ_3	λ_4
0.02273	0.0028440	0.0003741	2.86×10^{-5}

Table 2.6: Parameters for MOX50 waste

For the scoping calculations the thermal source terms are expressed in terms of linear thermal load density (w/m) considering the repository design. In our calculations the Super container design is considered for both VHLW and MOX50 wastes, the parameters are given in Table 2.7.

Wastes	tHM/canister	Linear thermal load density (axial)
MOX 50	0.45665	1 canister/6.216 m
VHLW	1.33	2 canisters/4.2 m

Table 2.7: Super container designs for PC case

The results of this conversion as a linear thermal density (w/m) are given in Figure 2.3.

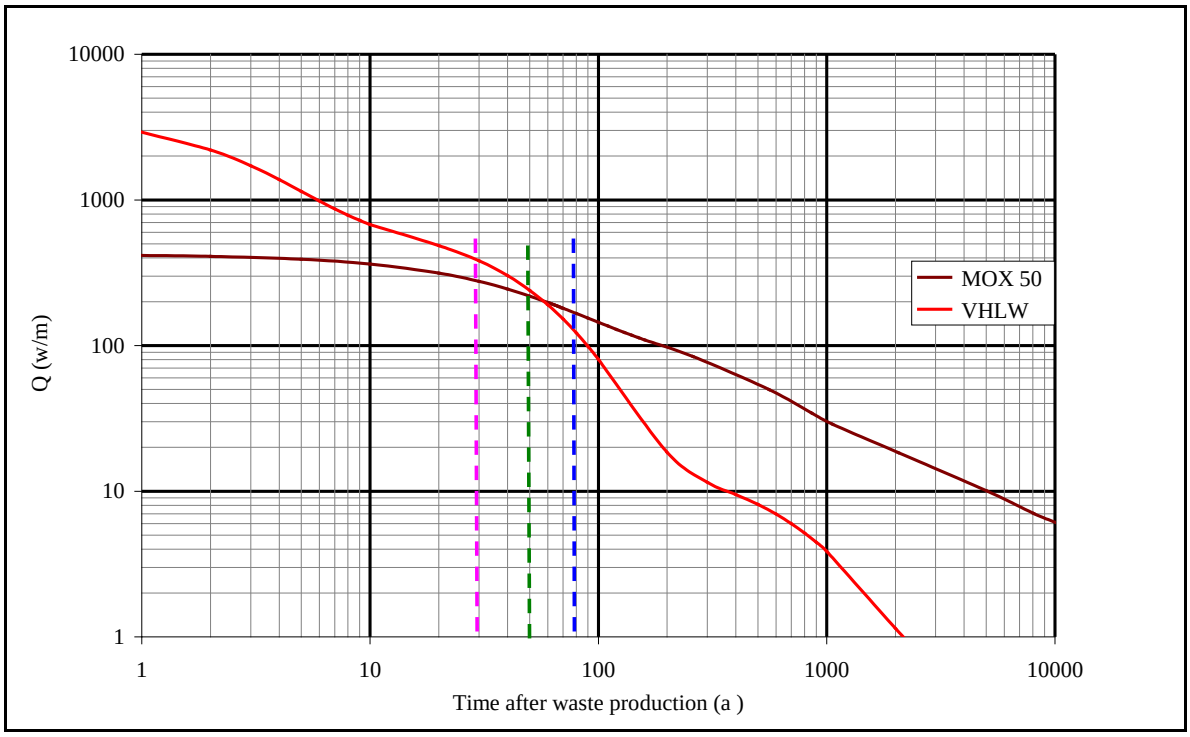

Figure 2.3: Evolution of linear thermal density for two types of waste after their produciton

2.6 Stages of Simulation

The general definitions used in the calculations are given below.

- Excavation Time: The total stress and pore pressure arer decreased linearly at the tunnel surface to atmospheric pressure in t_{exc} days.

  t_{exc}: 3 days (end time of excavation)

- Open Drift Time: The gallery is considered to be under drained condition after construction of the gallery during in t_{drain} days.

  t_{drain}: 1 year

- Heating Time: The canisters are assumed to be installed at the inner surface AB and a decreasing heat flux is given from this surface considering drained, undrained and dripping conditions in t_{heat} days.

  t_{heat}: 1000 years

3. STEADY STATE CONDITION

3.1 Long Term Constant Heat Flux Application

Before computing the case studies, a constant heat flux is applied to the tunnel surface to observe the evolution of temperature in the gallery. Q/b=240 (W/m) with λ=1.5 (W/m/K), is used as a constant heat flux and applied just after the end of open drift case till until 1500 years. The maximum temperature achieved during this constant heat flux is T_{max}: 131 ^{o}C. This value is compared to the value obtained by the equation given below. The agreement is good.

Steady State:

$$\Delta T = \frac{Q}{(2\times\pi\times\lambda\times b)}\ln(\frac{R}{R_0}) \rightarrow T_{Final} = 133^{o}C \qquad \text{(Eq.3.1)}$$

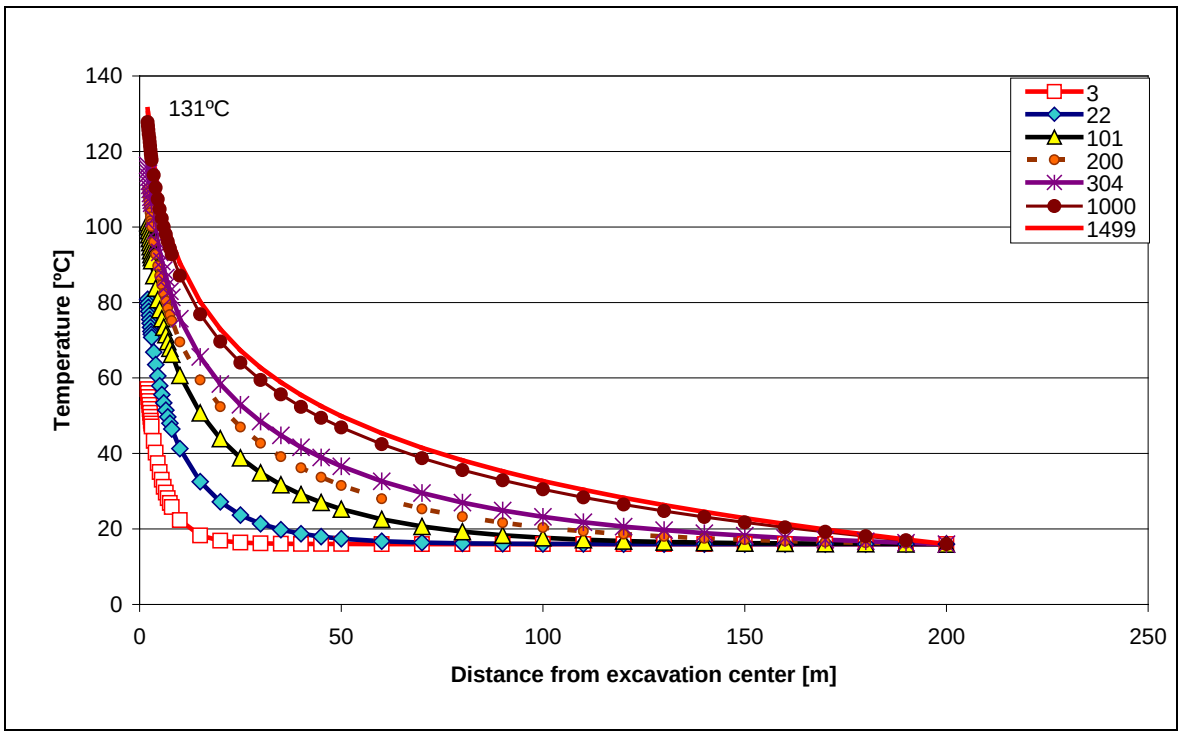

Figure 3.1: Temperature Evolution with Constant Heat Flux along the Radial distance at different periods

4. CASE STUDIES

4.1 Case I: Heating under Drained Condition

4.1.1 General Case

After the end of open drift time, heating starts and tunnel phase is supposed to be drained (i.e AB is a pervious surface) during heating. The pore water pressure at this boundary is fixed to be the atmospheric pressure. The duration of the heating is taken as mentioned 1000 years. Two different type of heat sources are applied after 50 years of cooling time on surface.

Temperature, pore pressure, displacement and stress phenomenon are investigated from beginning of the excavation and during heating of the gallery.

4.1.2 VHLW Results

4.1.2.1 Temperature

The initial temperature of the gallery is 16 ºC. The initial heat flux, Q_0: 19.07 W/m^2, is applied to the tunnel surface and progressively decreasing afterwards. The temperature of the rock mass starts to increase respectively up to certain time. The highest temperature is achieved almost at the 9th year of heating period as T_{max}: 64.6 ºC. Figure 4.1 shows the heat evolution during time at different radius from the center of gallery.

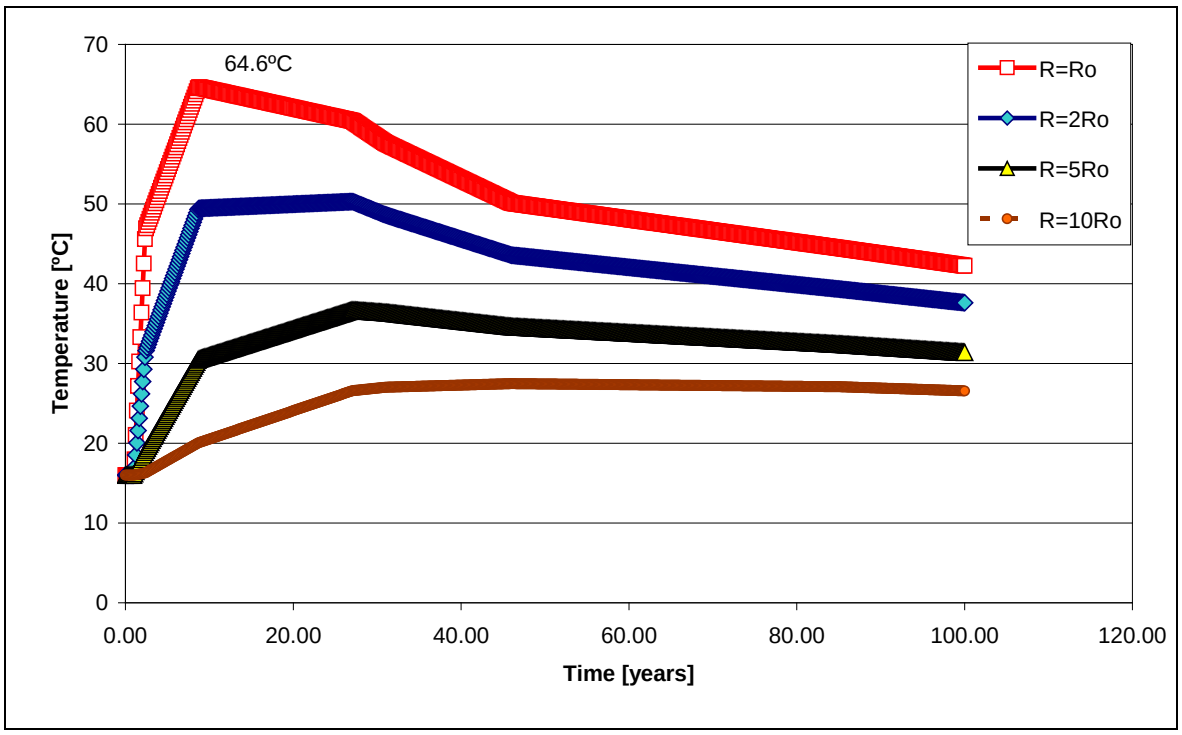

Figure 4.1: Temperature evolution at R=Ro

The temperature variation is observed almost in the first 100 m section (significant variation is observed in the first 25th m of the gallery). The radial profile of the temperature at different periods is given in Figure 4.2:

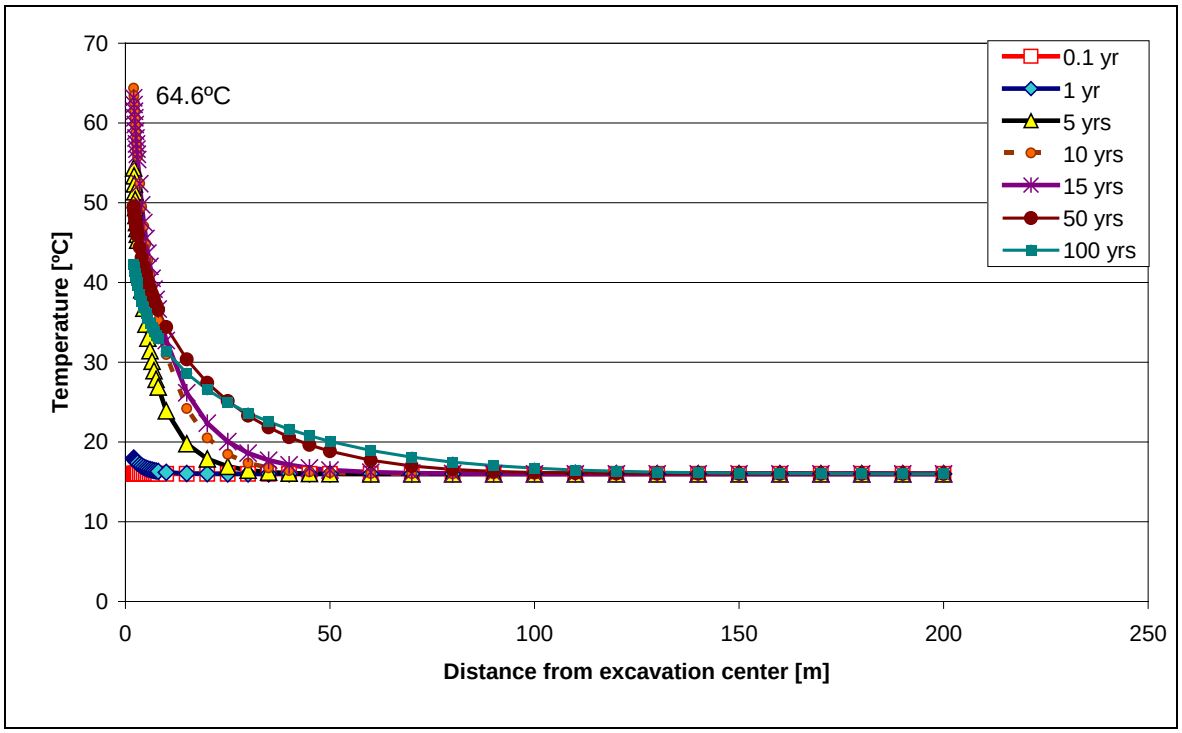

Figure 4.2: Radial profile of temperature at different periods

4.1.2.2 Liquid (Pore) Pressure

The radial profile of the pore pressure of the media at different periods is given in Figure 4.3. As stated before the pore pressure decreases linearly to atmospheric pressure during excavation. During heating, up to achieving T_{max}, temperature and pore pressure increase near the gallery wall due to the differential dilation of water, grains and skeleton. The drained condition of the tunnel surface has an important influence during heating.

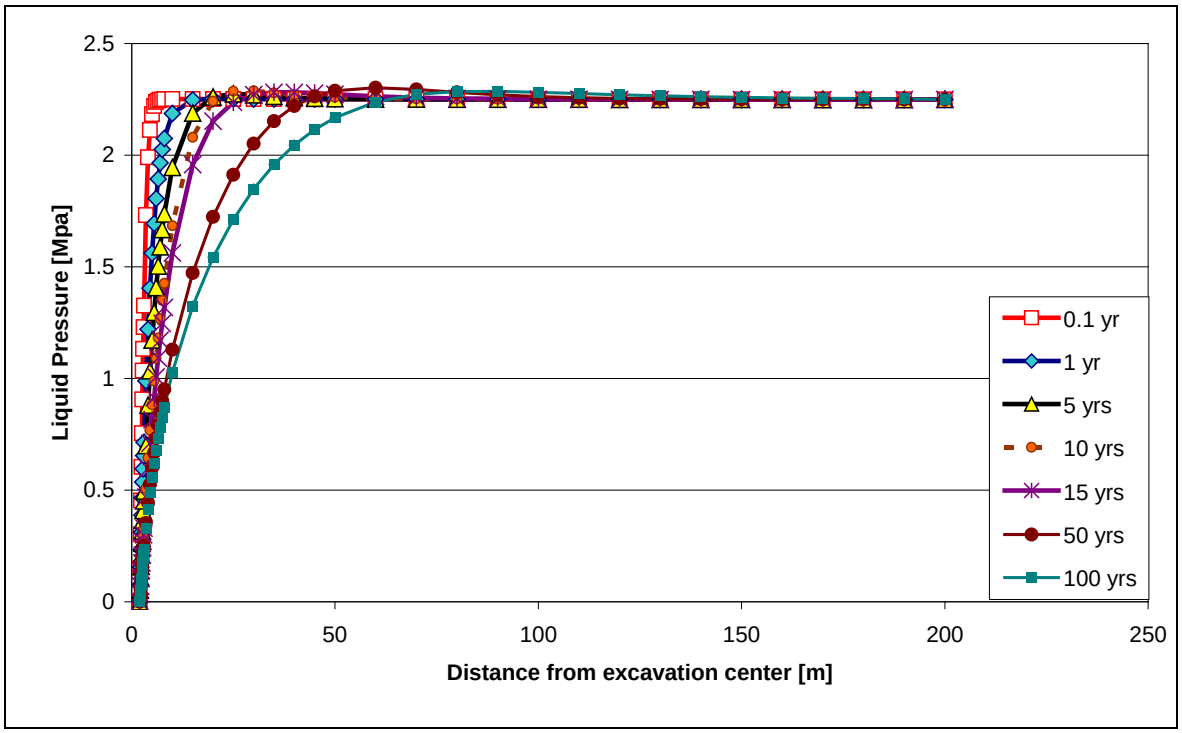

Figure 4.3: Radial profile of pore pressure at different periods

4.1.2.3 Displacements

When releasing total stresses by excavating the tunnel surface, a negative displacement of 3.36 cm is observed in the gallery. This behavior continues in the open drift period. After applying the heat flux, there is a decrease in the increment of negative displacements up to 15 years. Between 15-40 m negative displacements are higher than the initial ones for longer heating periods. Figure 4.4 and 4.5 shows the radial displacements and strain compositions at different periods.

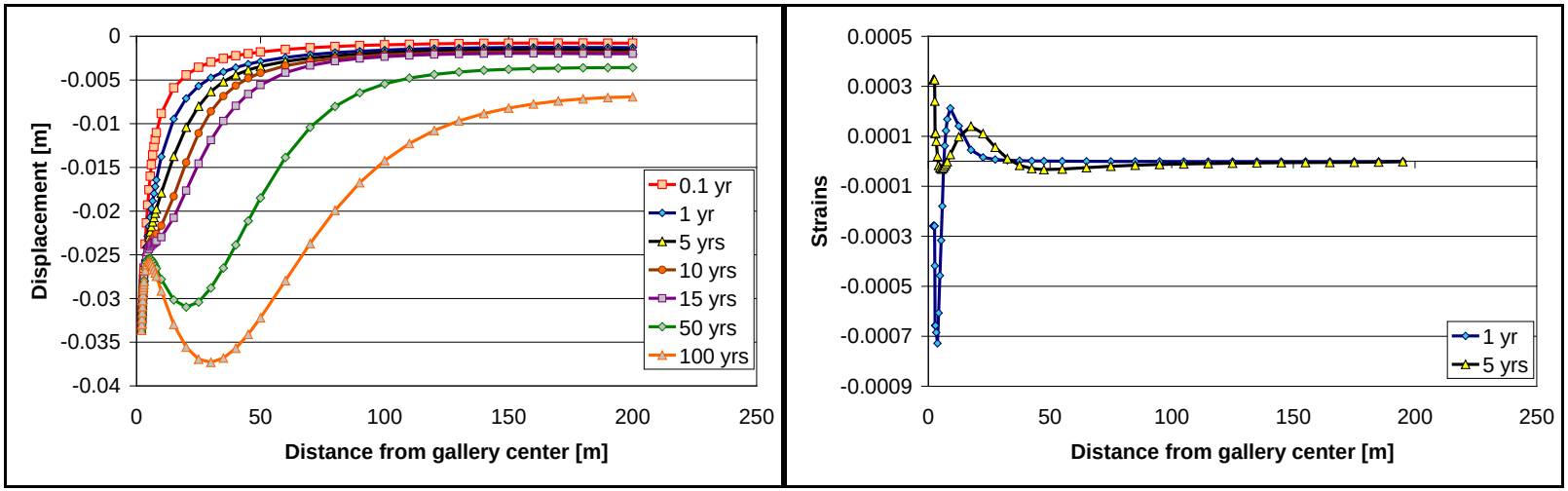

Figure 4.4: a) Radial profile of displacements at different periods b) Strains due to heating at 1and 5 years

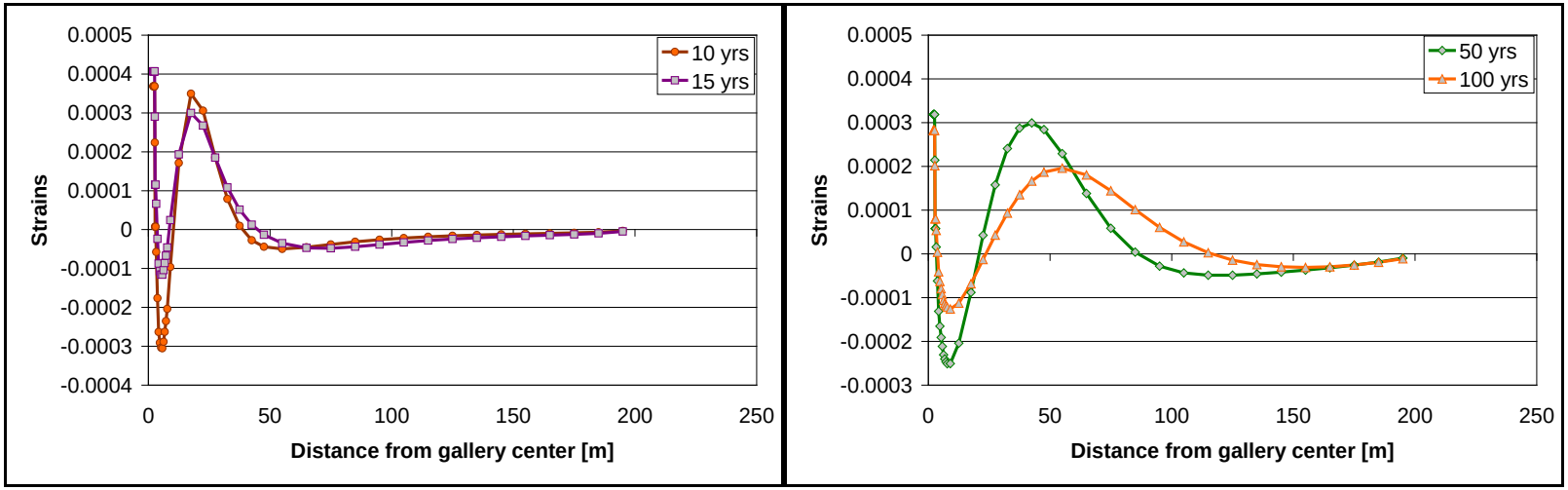

Figure 4.5: a) Strain composition at 10 and 15 years b) Strains due to heating at 50 and 100 years

4.1.2.4 Stresses

The total radial stress and circumferential stress profile at different periods are shown in Figure 4.6 and 4.7 respectively.

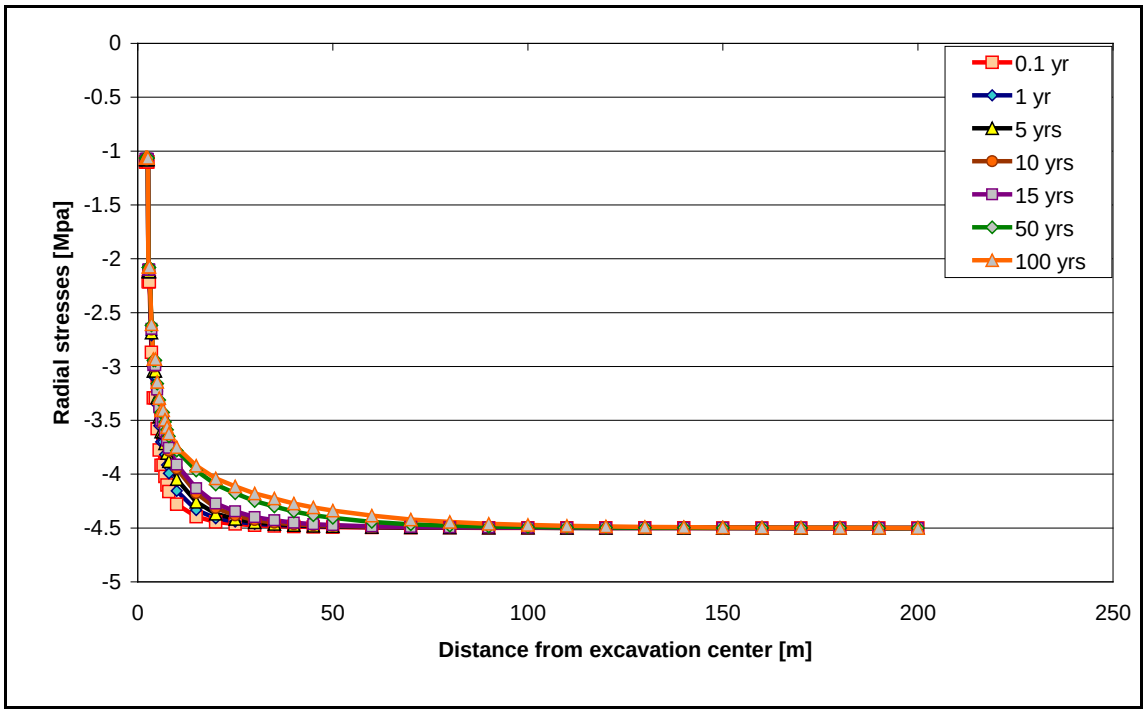

Figure 4.6: Radial profile of Stresses at different periods

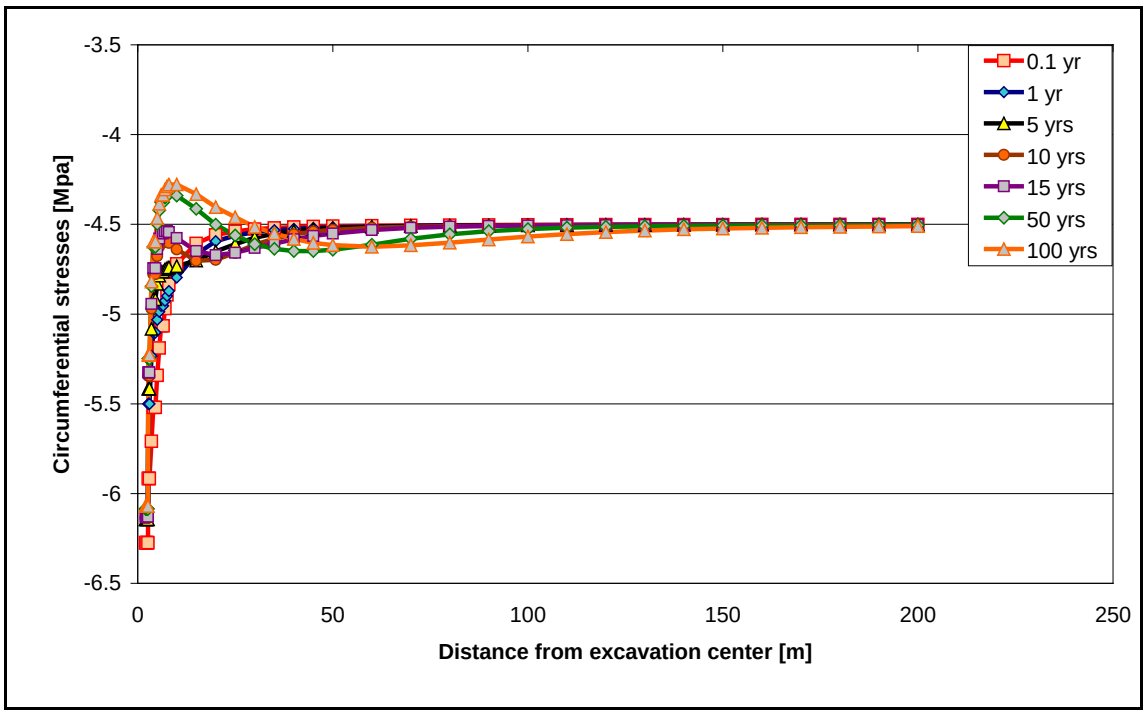

Figure 4.7: Radial profile of circumferential stresses at different periods

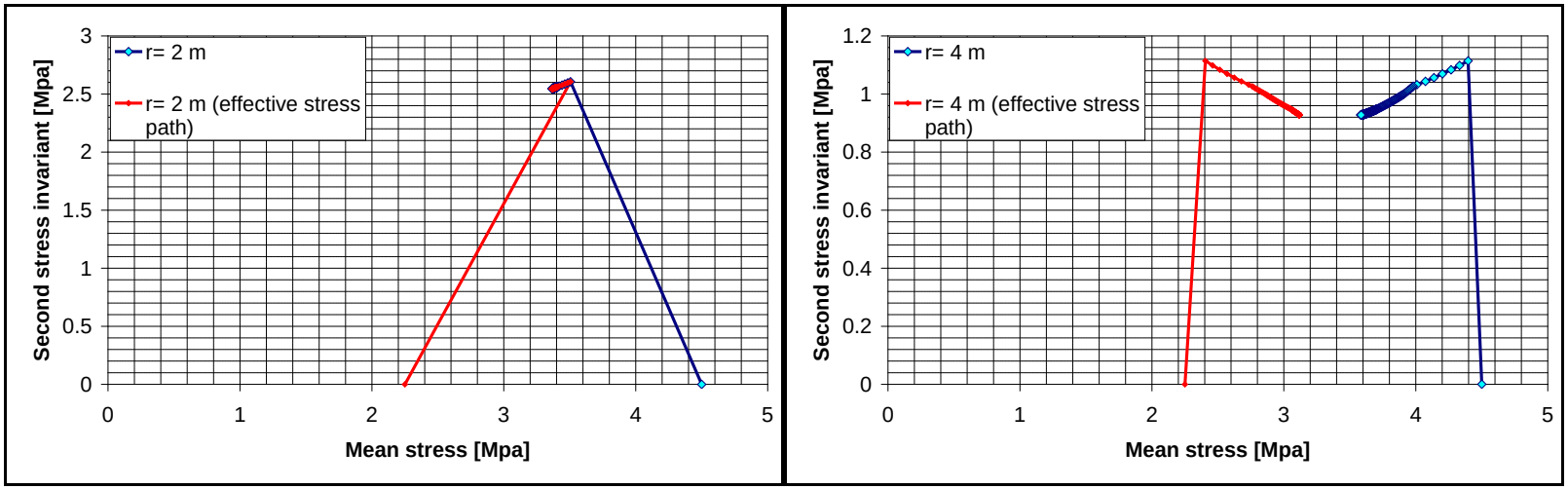

Figure 4.8: Effective and total stress paths at r = R_0, r = $2R_0$,

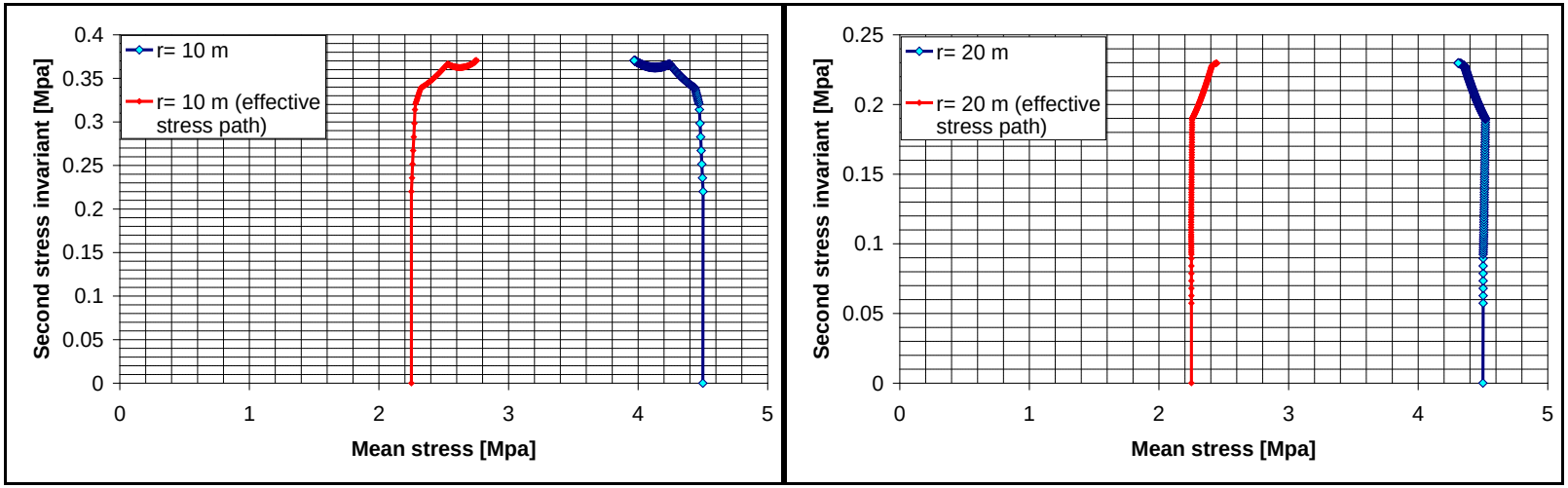

Figure 4.9: Effective and total stress paths at r = $5R_0$ and r = $10R_0$

The total and effective mean stress path of clay at different radius r = R_0, 2 R_0, 5R_0 and 10 R_0 in the (p', q) stresses plane are shown in Figure 4.8 and Figure 4.9.

4.1.3 MOX50 Results

MOX50 thermal source is also applied after 50 years of cooling time on surface. The heating duration is taken 1000 years.

4.1.3.1 Temperature

The initial flux, Q_0: 15.22 W/m^2, is applied to the tunnel surface and progressively decraesed. The highest temperature (T_{max}: 63.5 ^oC) is achieved almost at 70 years of heating. The heat generation inside R=10 R_0 section of the gallery in MOX50 case is higher than in VHLW case at the end of 100 years. Figure 4.10 shows the heat evolution with time at different radius from the center of gallery in MOX50.

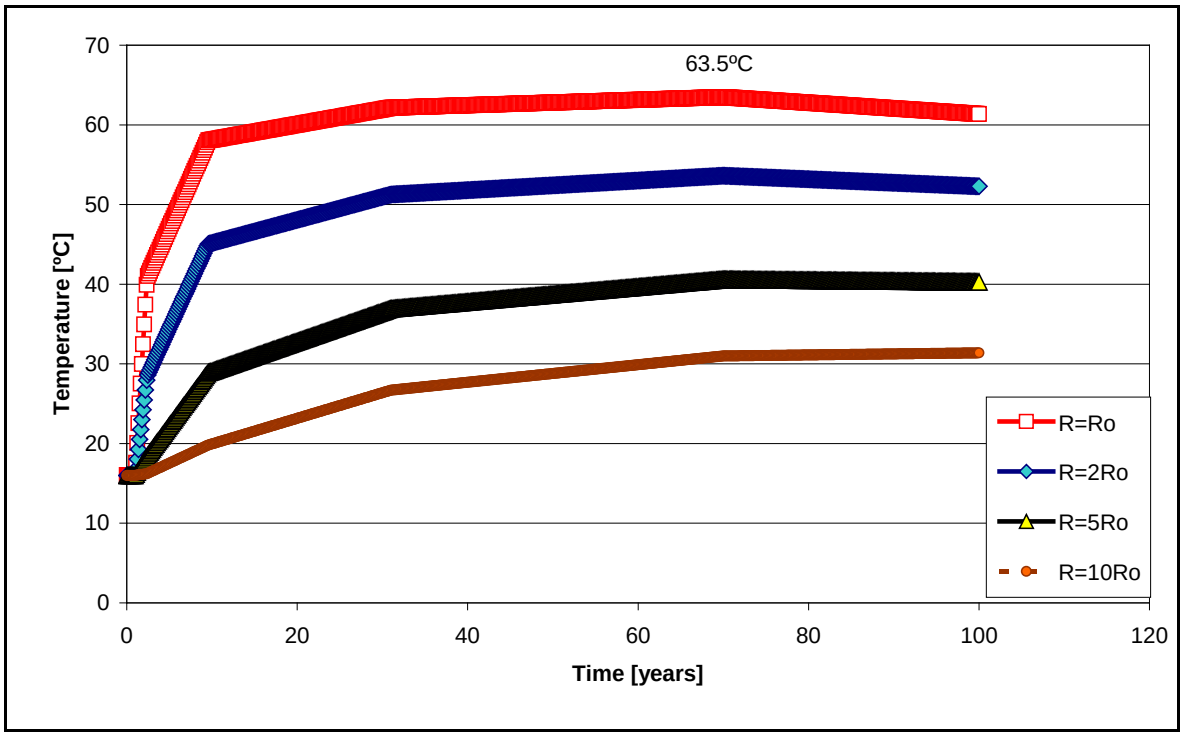

Figure 4.10: Temperature evolution at R=Ro in MOX50 case

4.1.3.2 Pore Pressure

The trend of the pore pressure variation in MOX50 waste case is almost similar to VHLW waste case. The rise of temperature induces a reduction of pore space, which causes an increase of water pressure. After this period, as the temperature decreases until returning to its initial state, the pore water pressure drops. Figure 4.11 shows the radial profile of pore pressure at different periods in MOX50 waste case.

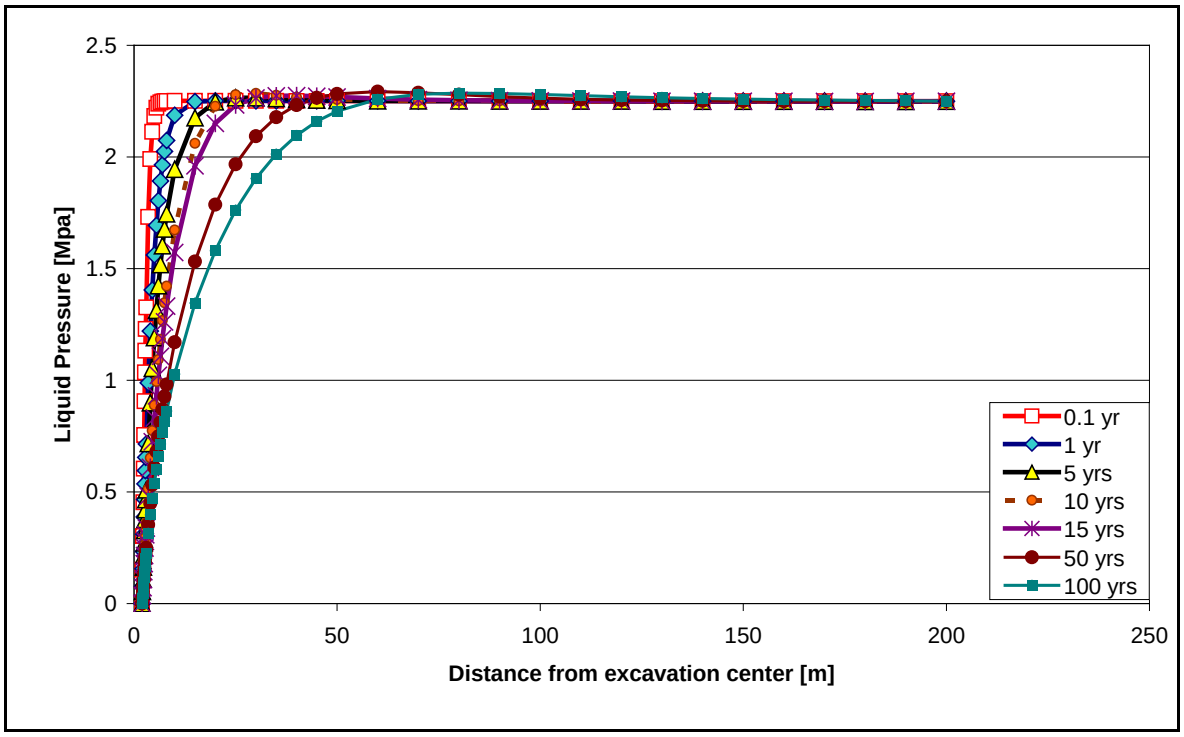

Figure 4.11: Radial profile of pore pressure at different periods in MOX50 waste case

4.1.3.3 Displacements

The tendency of the displacement is the same with VHLW waste case. Figure 4.12 shows the radial displacements at different periods in MOX50 waste case.

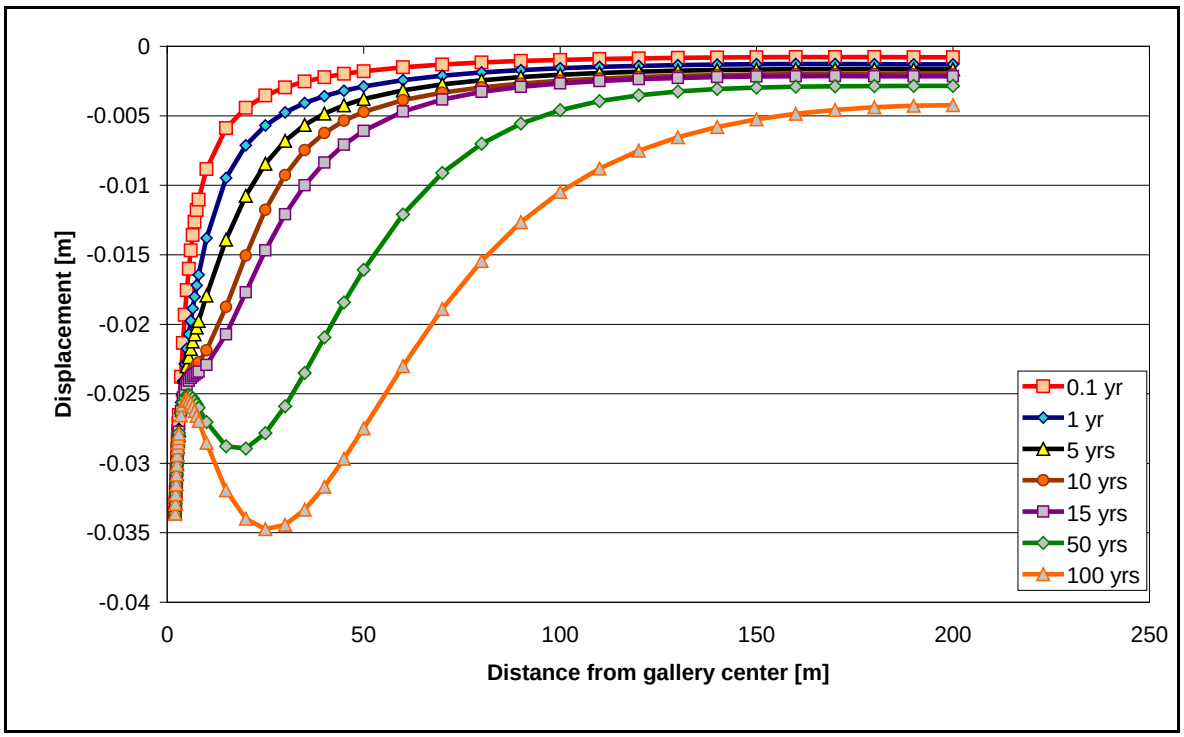

Figure 4.12: Radial profile of displacements at different periods in MOX50 waste case

4.2 Case II: Heating under Undrained Condition

4.2.1 General Case

The drained condition of the tunnel surface is maintained till the end of open drift period, on the start of heating, the tunnel face is assumed undrained (i.e. AB surface is impermeable) and heat flux is applied considering this undrained condition. The pore water pressure at this boundary is no longer fixed to be the atmospheric pressure. During 1000 years of heating period, heat flux of **VHLW** waste is applied after 50 years of cooling time on surface.

Temperature, pore pressure, displacement and stress phenomenon are studied.

4.2.2 Temperature

The evolution of the temperature in undrained condition shows the same trend as in drained condition. There is an increase of temperature up to T_{max}: 64.8 ^{o}C for 10 years and then it starts to decrease to almost its initial condition at the end of heating period.

4.2.3 Pore Pressure

The evolution of the pore pressure in the undrained case is the same as in the excavation and open drift time periods as in drained case. During heating, the pore pressure increases with time due to the undrained condition of the rock mass. Figure 4.13 shows the pore pressure distribution at different periods.

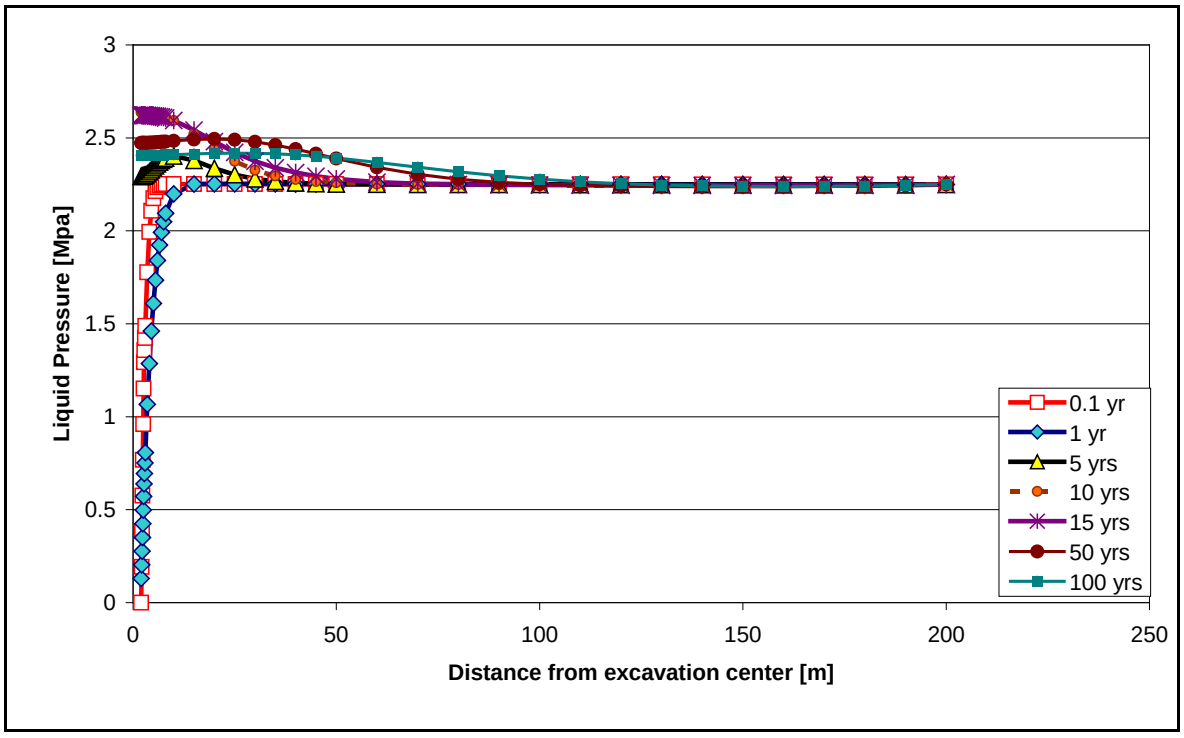

Figure 4.13: Radial profile of pore pressure at different periods in undrained case

4.2.4 Displacements

Figure 4.14 shows the radial profile of displacements at different periods in the undrained case. As it can be seen in the figure, positive displacements are obtained starting from the first 10 meter of the gallery until the outer end of the domain due to the increment of the temperature and pore pressure in the undrained case.

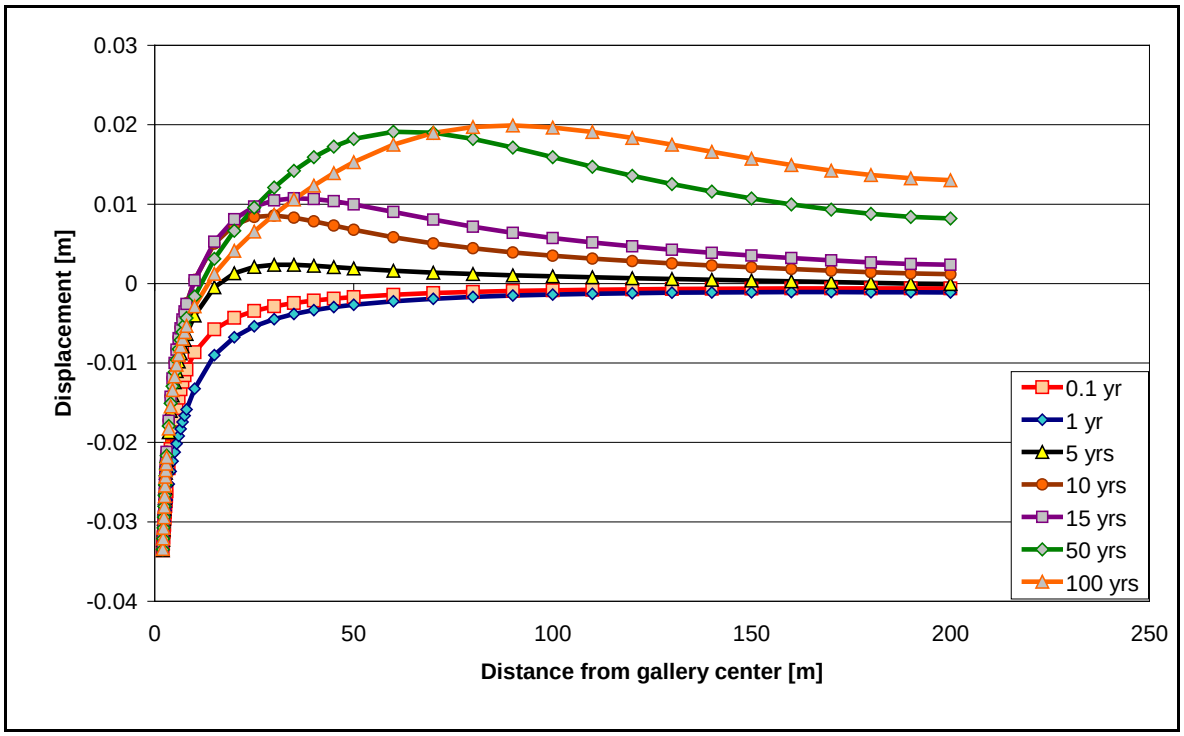

Figure 4.14: Radial profile of displacements at different periods in undrained case

4.2.5 Stress Paths

Figure 4.15 and 4.16 show the radial profile of radial stresses and circumferential stresses at different periods in undrained case respectively.

The effective and total mean stress paths of clay at different radius r = R_0, 2 R_0, 5R_0 and 10 R_0 in the (p', q) stresses plane are shown in Figure 4.17.

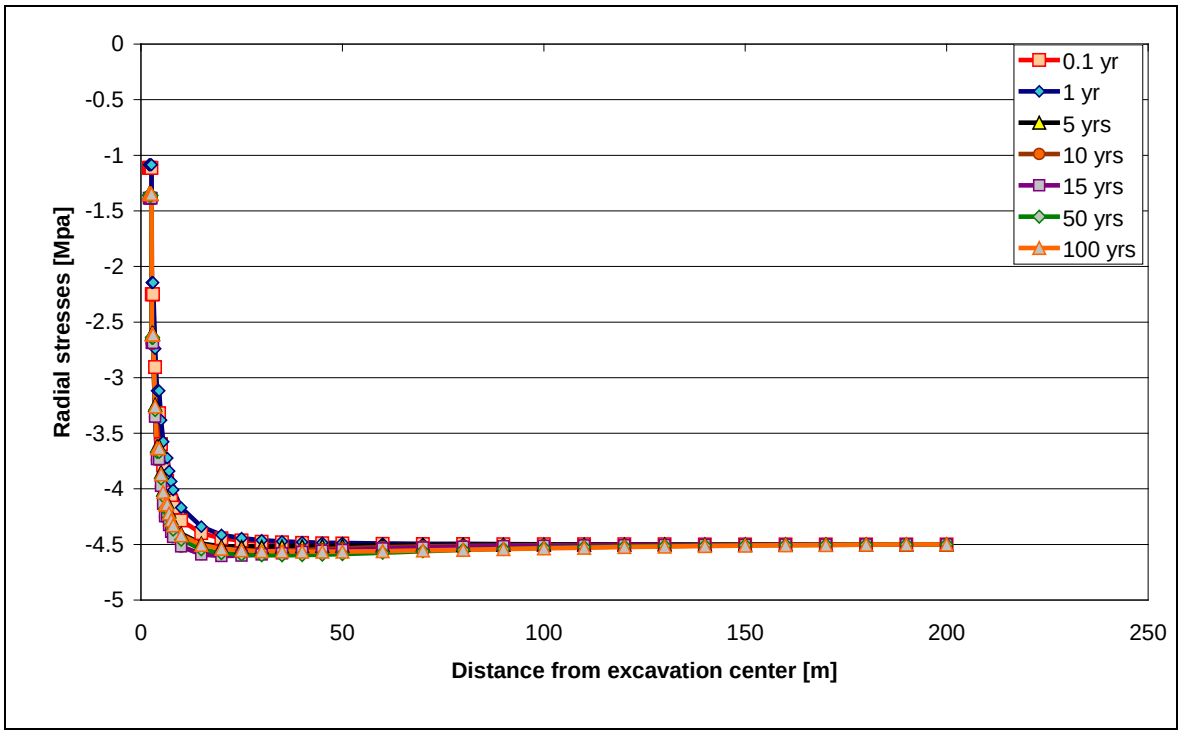

Figure 4.15: Radial profile of radial stresses at different periods in undrained case

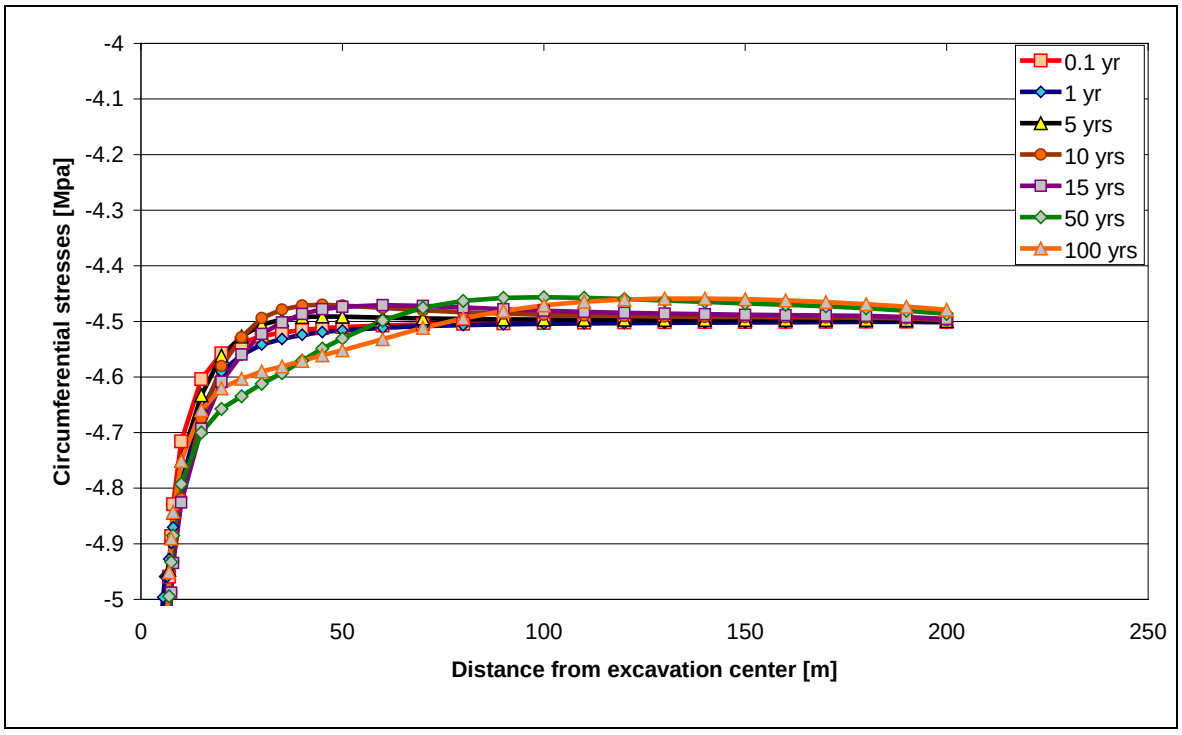

Figure 4.16: Radial profile of circumferential stresses at different periods in undrained case

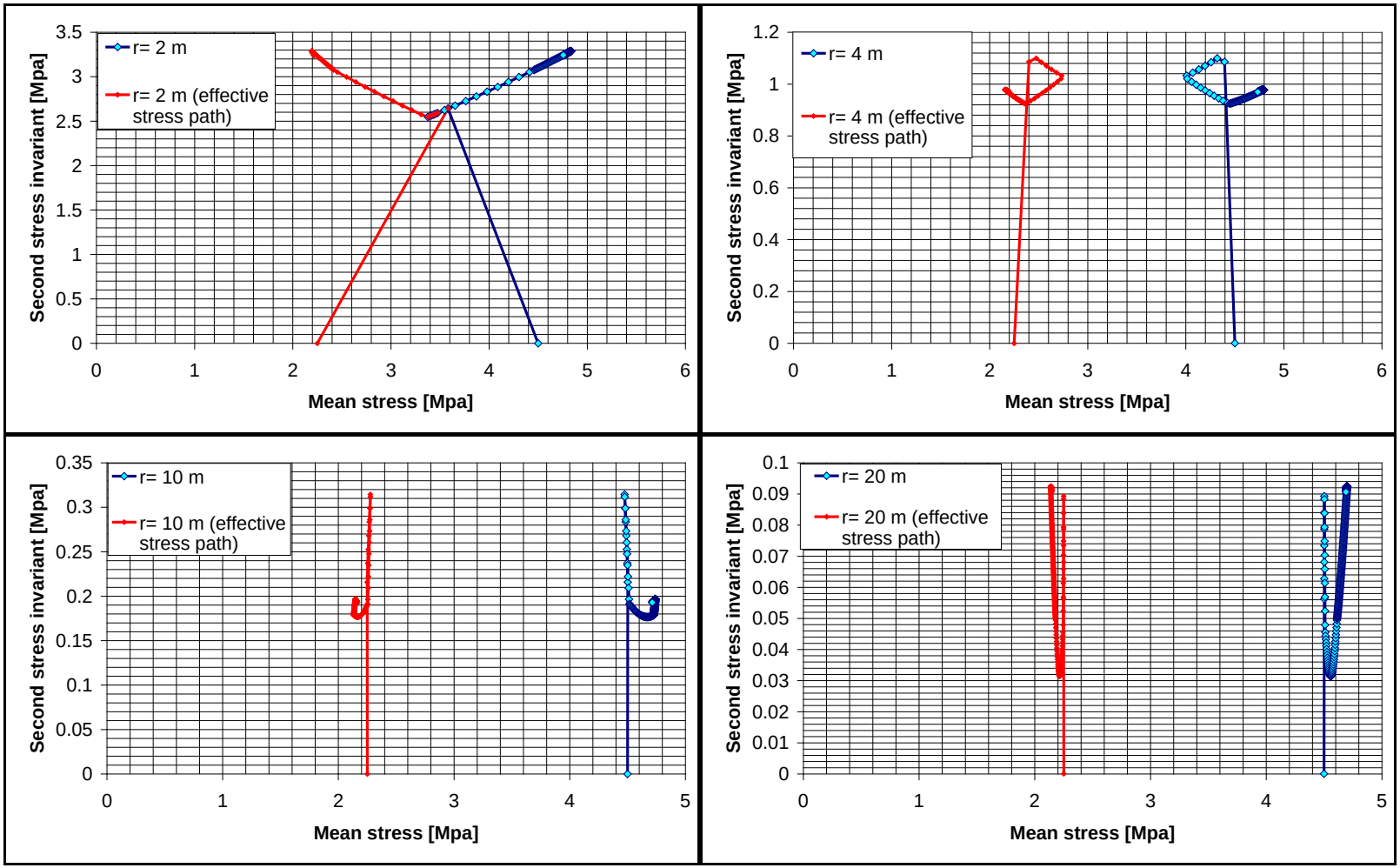

Figure 4.17: Effective and total stress paths at r = R_0, r = $2R_0$, r = $5R_0$ and r = $10R_0$

4.3 Case III: Heating under Dripping Condition

4.3.1 General Case

A more realistic hydraulic condition is a dripping boundary condition: a water flow can exist only if the pore pressure in the formation is greater than the atmospheric pressure as shown in Figure 4.18.

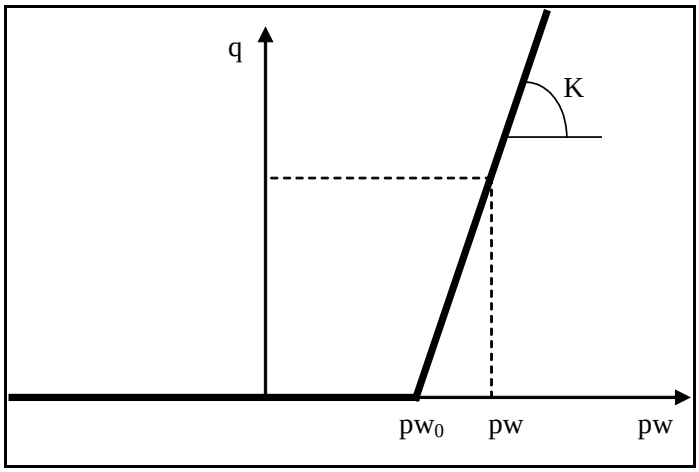

Figure 4.18: Dripping condition

where q : output or input flow at the boundary

K : a penalty coefficient

if $p_w < p_{w0}$: $q = 0$

if $p_w > p_{w0}$: $q = K (p_{w0} - p_w)$

p_{w0} is equal to the air pressure in the gallery

In this case, the dripping tunnel surface condition is prescribed from the start of heating. Water flow will occur only when the pore pressure is larger than the atmospheric pressure.

4.3.2 Temperature

The evolution of the temperature in the dripping case shows the same trend as in drained case. There is an increase of temperature up to T_{max}: 64.6 ^{o}C until the end of the 9th year and then it starts to decrease to almost its initial condition at the end of heating period.

4.3.3 Pore Pressure

The radial profile of the pore pressure of the domain at different periods is given in Figure 4.19. The trend obtained in the dripping case is similar to the drained case.

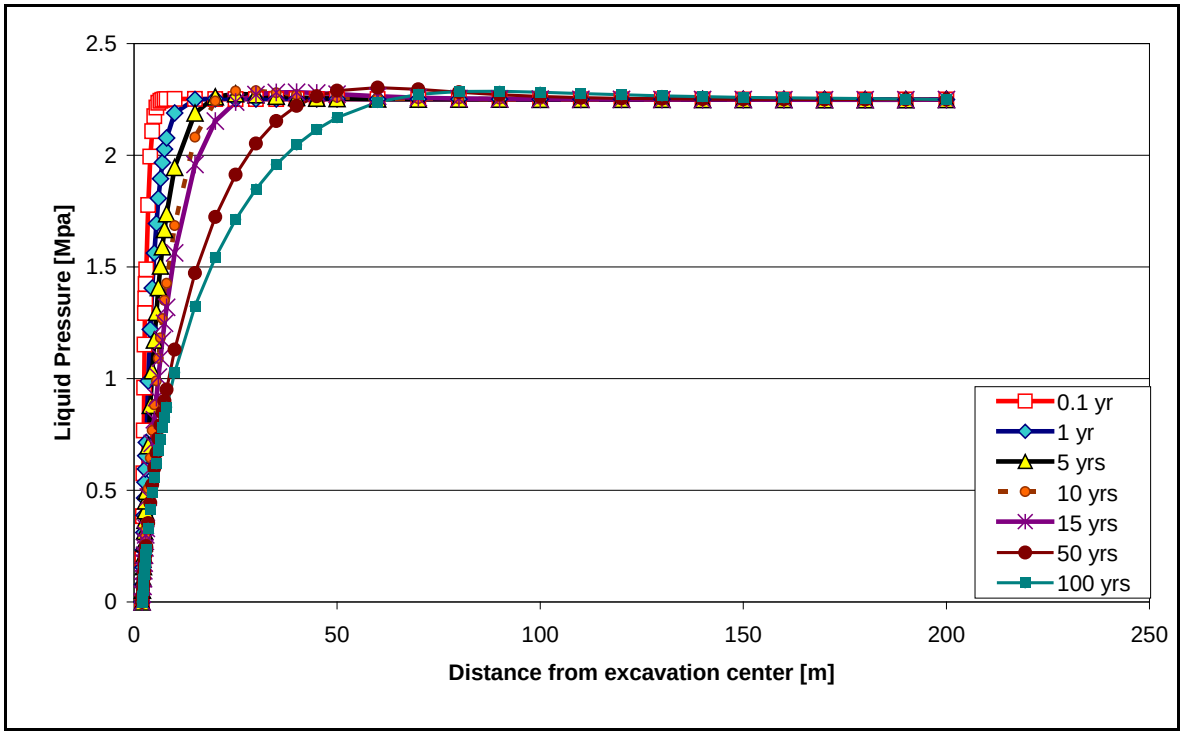

Figure 4.19: Radial profile of pore pressure at different periods in dripping case

4.3.4 Displacements

As in the drained case, when releasing the total stresses by excavation, a 3.36 cm negative displacement is observed in the gallery. The trend is similar as in the drained case.

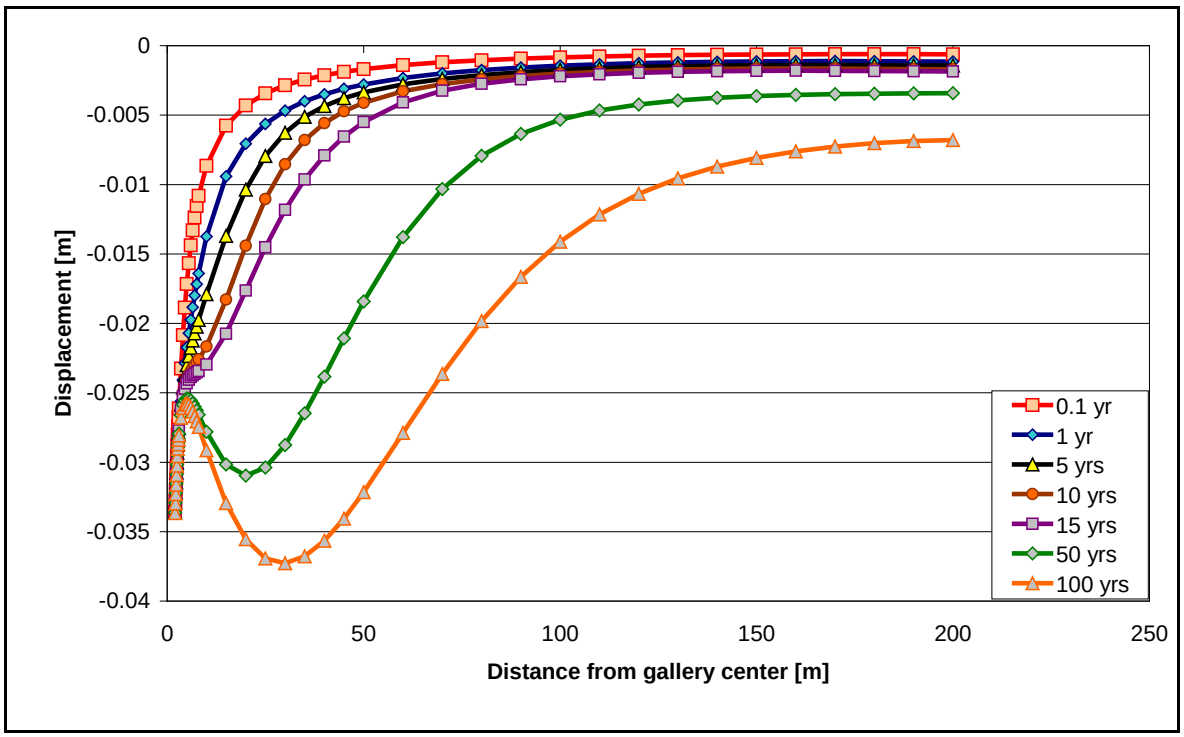

Figure 4.20: Radial profile of displacements at different periods in dripping case

4.3.5 Stress Paths

The total radial stress and circumferential stress profile at different periods are shown in Figure 4.21 and 4.22 respectively. Also the total and effective mean stress path of clay at different radius r = R_0, 2 R_0, 5 R_0 and 10 R_0 in the (p`,q) stress plane are shown in Figure 4.23.

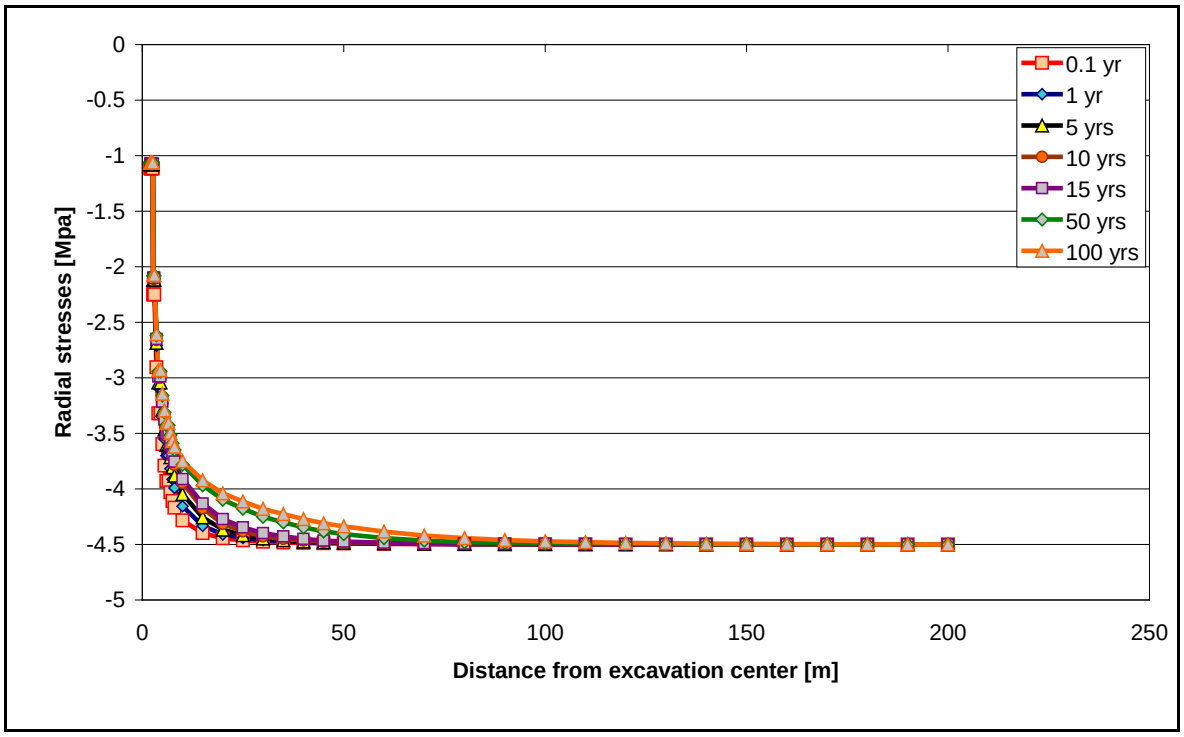

Figure 4.21: Radial profile of radial stresses at different periods in dripping case

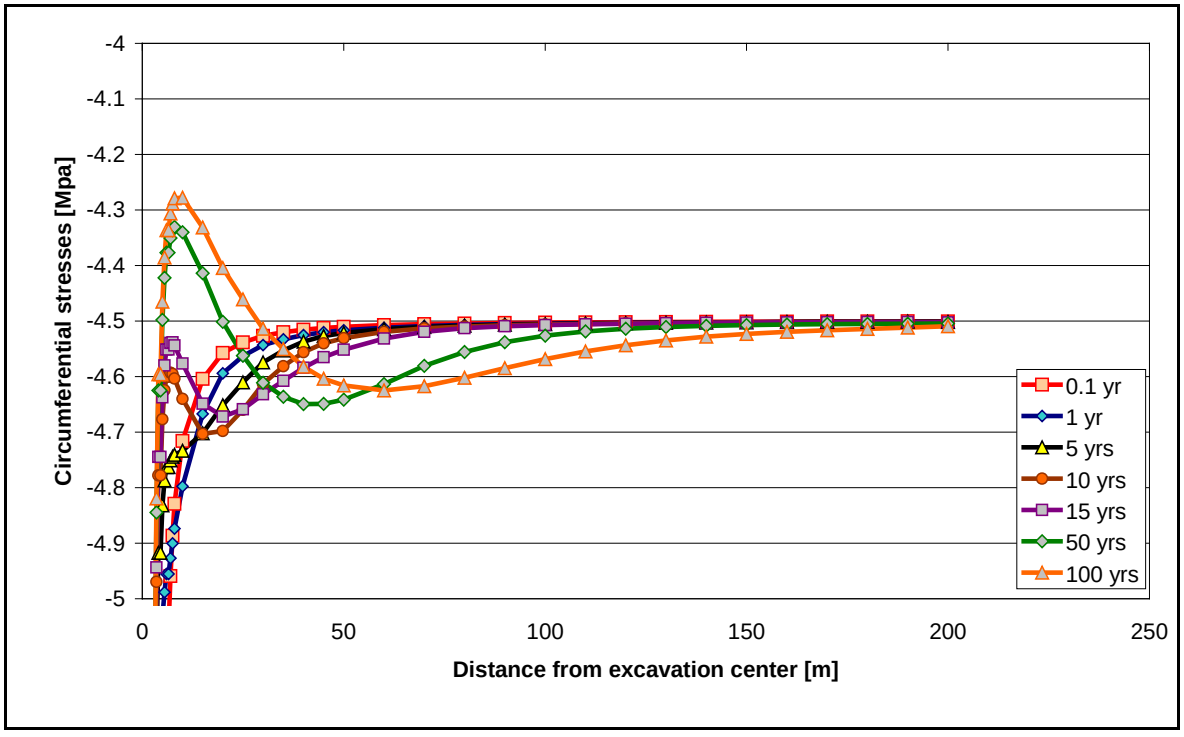

Figure 4.22: Radial profile of circumferential stresses at different periods in dripping case

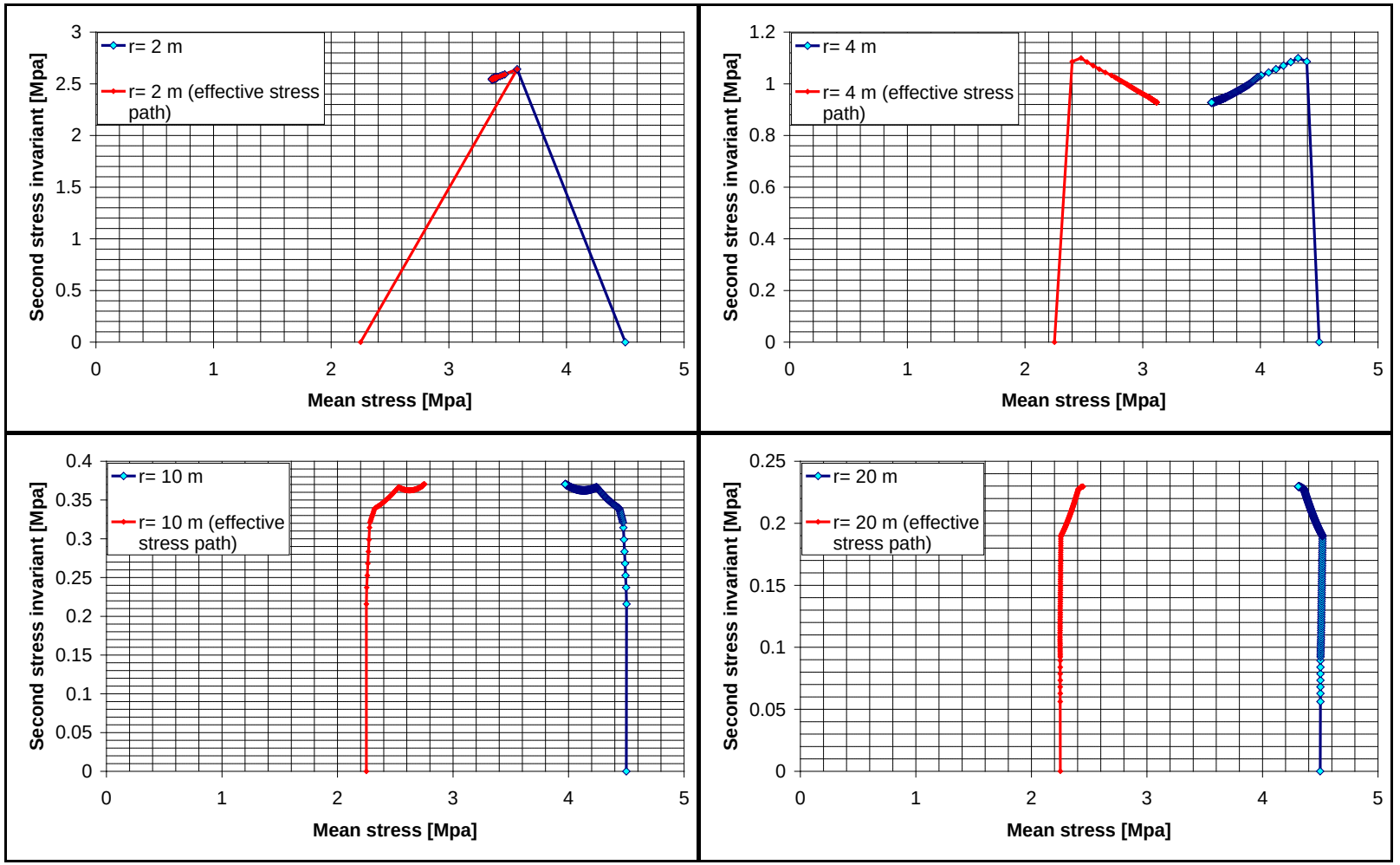

Figure 4.23: Effective and total stress paths at r = R_0, r = $2R_0$, r = $5R_0$ and r = $10R_0$

5. SENSITIVITY ANALYSES

An additional study has been performed to clarify the effect of the uncertainties of some parameters. Table 5.1 presents the parameters that are examined in this section.

Parameters	VHLW drained	MOX50 Drained	VHLW undrained
Thermal Conductivity (W/m/K)	**1.35 / 1.7** (Lower and upper boundaries)		
Intrinsic Permeability (m^2)		**$1*10^{-19}/1*10^{-20}$**	**$1*10^{-19}/1*10^{-20}$**

Table 5.1: Parameters studied on the sensitivity

5.1 Thermal Conductivity - VHLW Drained Condition

The effect of the thermal conductivity is studied in the case of VHLW waste in drained condition. The thermal conductivity coefficients are chosen as the lower, middle and upper values of the given thermal coefficient interval.

As seen in the Figure 5.1 and shown in Table 5.2; when the material is less conductive (reducing the thermal coefficient), a higher temperature is achieved. Increasing the thermal coefficient reduces the temperatures. The maximum temperatures are obtained almost at the same time value and the radial distributions of temperature are very similar (Figure 5.2)

	T_{max} (°C)	t (years)
λ = 1.35 W/m/K	68.7	9
λ = 1.50 W/m/K	64.6	9
λ = 1.70 W/m/K	60.1	9

Table 5.2: Maximum Temperatures obtained for different thermal conductivity values

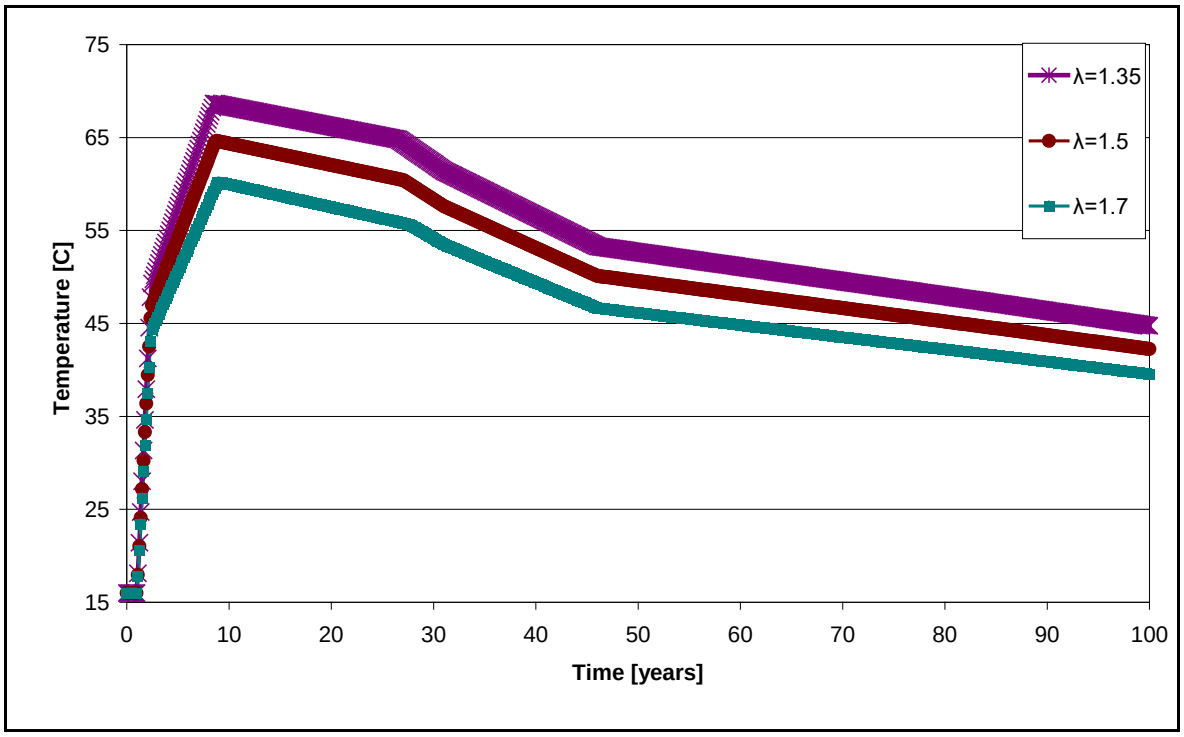

Figure 5.1: Temperature evolution at R=Ro for different thermal coefficients for VHLW drained condition

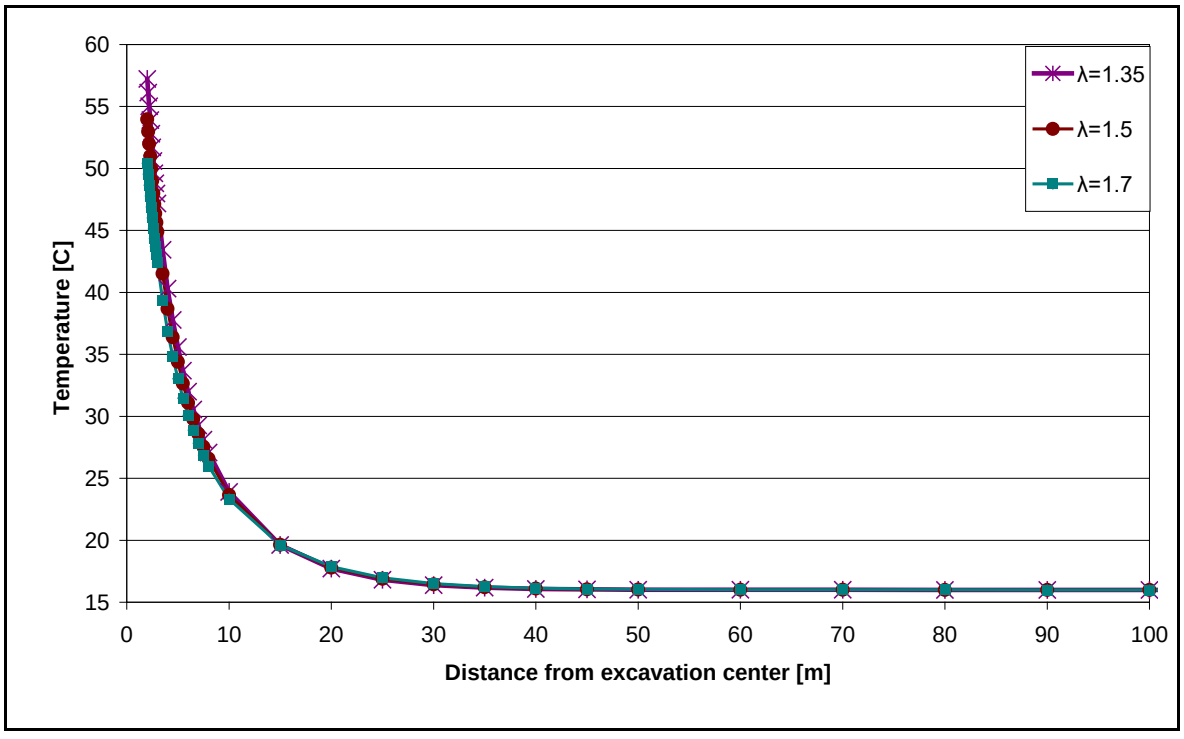

Figure 5.2: Radial profile of temperature for different thermal coefficients for VHLW drained condition

5.2 Intrinsic Permeability - MOX50 Drained Condition

The effect of hydraulic parameters is studied for the MOX50 drained case. The intrinsic permeability coefficients are chosen to be $1*10^{-19}$ and $1*10^{-20}$ m^2.

The variation of permeability mainly influences the pore pressure and, consequently, the effective stresses. There is no influence on the variation of temperature. As Figure 5.3 and 5.4 show; when the medium is less permeable the pore pressure generated in this porous medium is higher.

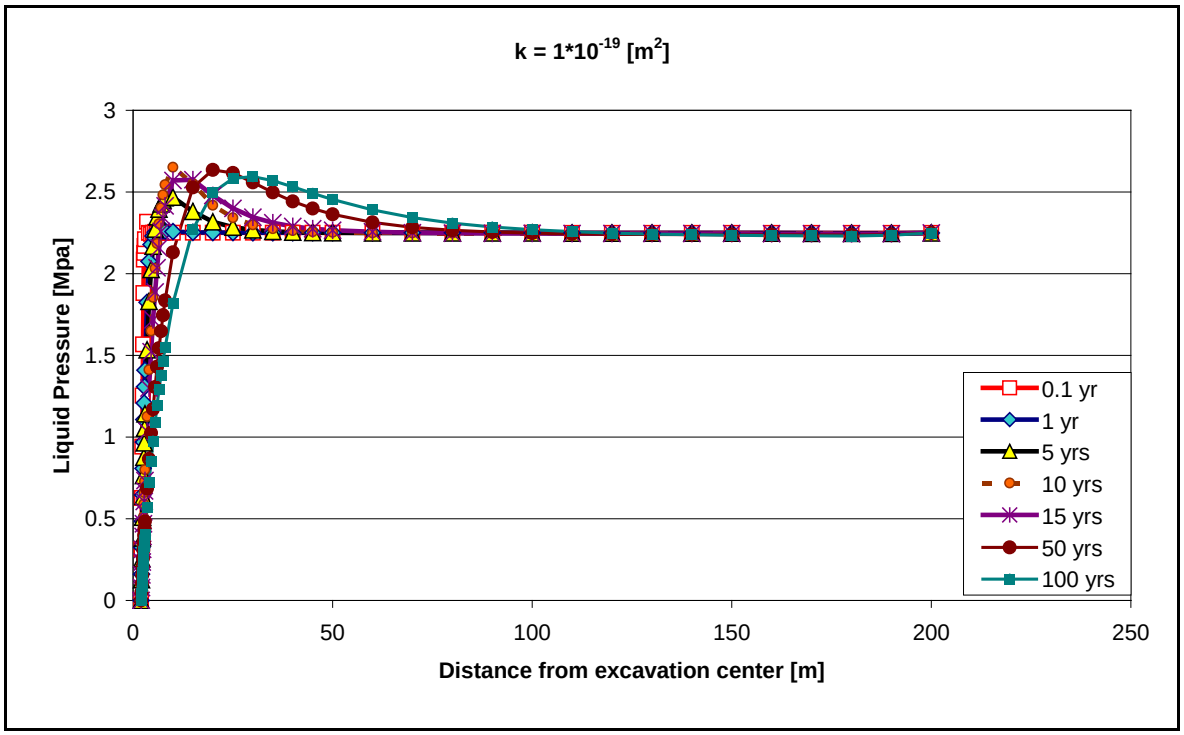

Table 5.3: Radial profile of pore pressure at different periods with k = $1*10^{-19}$ m^2 MOX50 drained condition

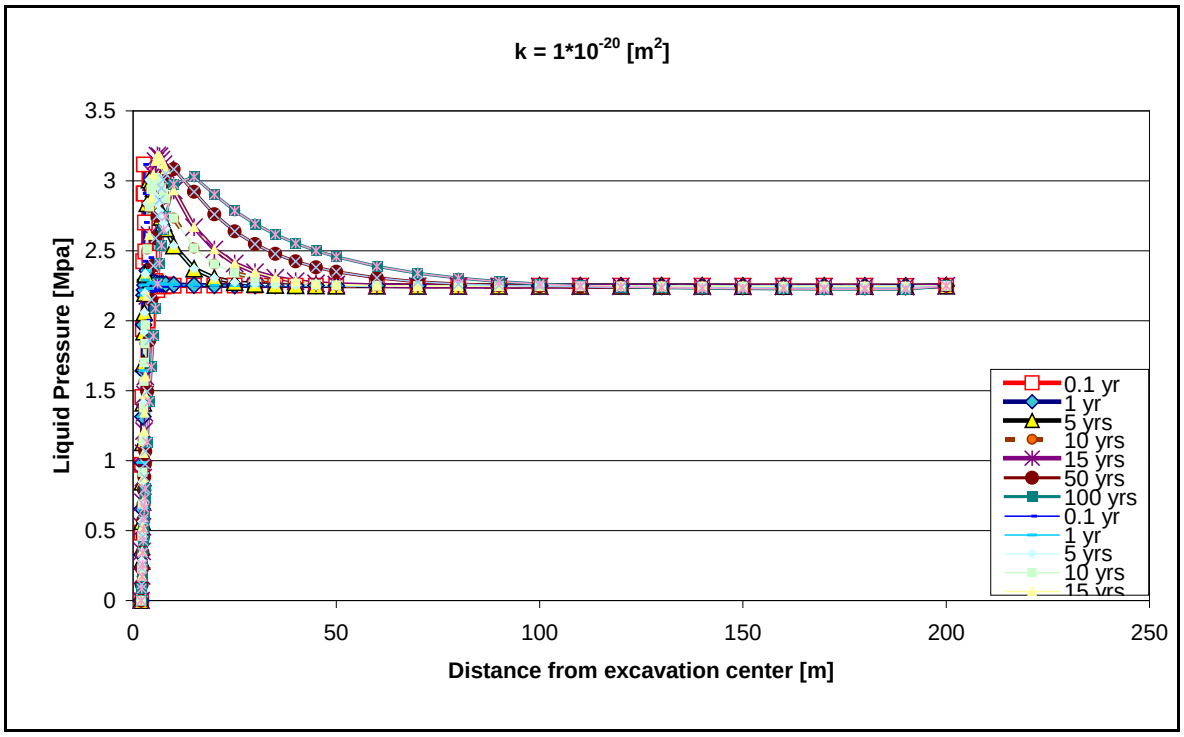

Table 5.4: Radial profile of pore pressure at different periods with k = $1*10^{-20}$ m^2 MOX50 drained condition

5.2 Intrinsic Permeability - VHLW Undrained Condition

As it was observed in drained condition, the variation of permeability mainly influences the pore pressure and effective stresses. When the medium is less permeable the pore pressure created in the porous medium is higher but this increment is larger than in the drained case due to the effect of the undrained condition.

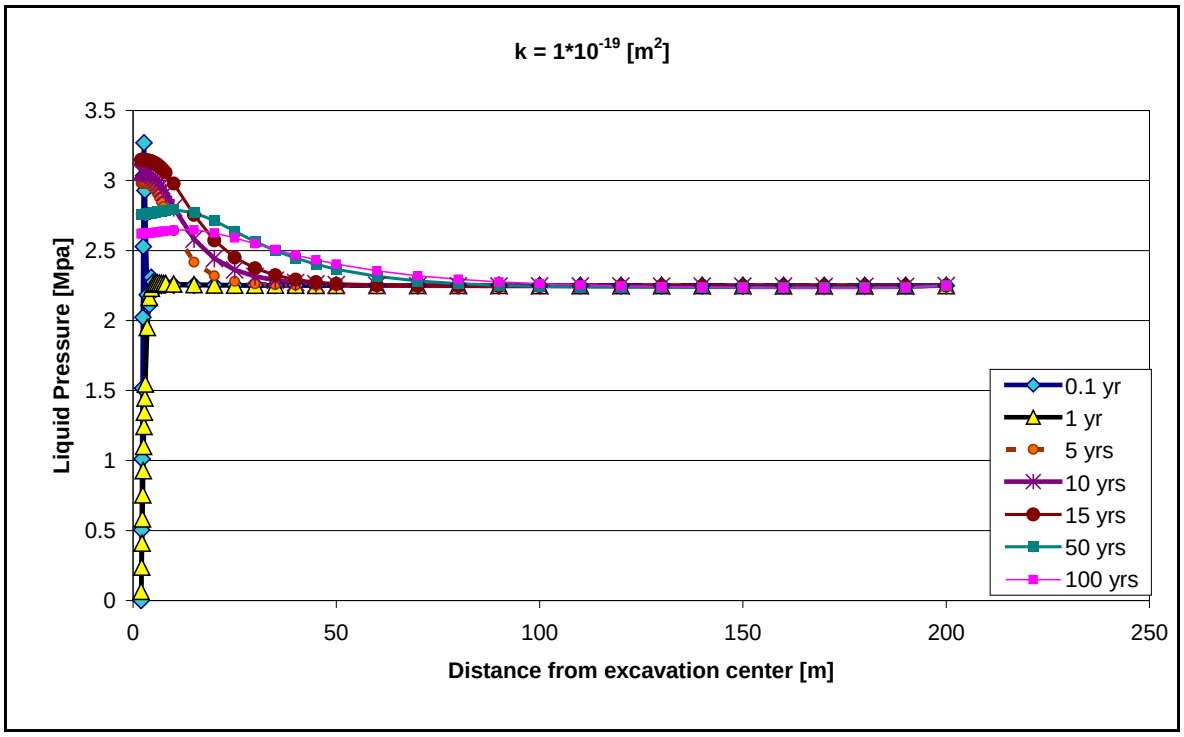

Table 5.5: Radial profile of pore pressure at different periods with k = $1*10^{-19}$ m^2 VHLW undrained condition

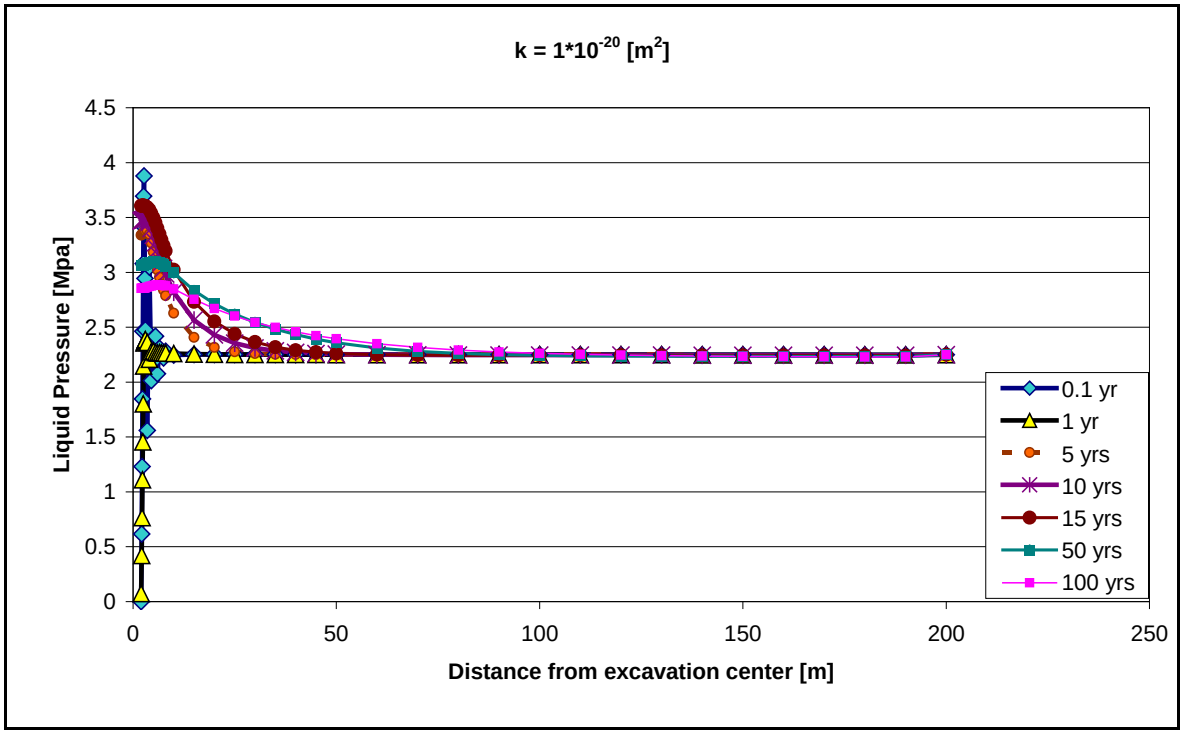

Table 5.6: Radial profile of pore pressure at different periods with k = $1*10^{-20}$ m^2 VHLW undrained condition

6. CONCLUSION

Some scoping calculations have been performed to enhance the insight on the effects of some parameters and boundary conditions on some relevant variables of the rock. In this study only the PC (plastic clay) case has been examined. Specifically, the effects of heat source, hydraulic boundary condition, thermal conductivity and hydraulic conductivity have been studied.